

Combining spatial information sources while accounting for systematic errors in proxies

Christopher J. Paciorek

Department of Biostatistics, Harvard School of Public Health, Boston, USA, and
Department of Statistics, University of California, Berkeley, USA

November 13, 2021

Abstract

Environmental research increasingly uses high-dimensional remote sensing and numerical model output to help fill space-time gaps between traditional observations. Such output is often a noisy proxy for the process of interest. Thus one needs to separate and assess the signal and noise (often called discrepancy) in the proxy, given sparse observations and complicated spatio-temporal dependences. Here I extend a popular two-likelihood hierarchical model using a more flexible representation for the discrepancy. I employ the little-used Markov random field approximation to a thin plate spline, which can capture small-scale discrepancy in a computationally efficient manner, while better modeling smooth processes than standard conditional auto-regressive models. I apply the approach to spatio-temporal mapping of fine particulate matter (PM) air pollution using satellite aerosol and atmospheric model output proxies. The estimated discrepancies occur at a variety of spatial scales, with small-scale discrepancy particularly important. The examples indicate little predictive improvement over modeling of the observations alone, which is also seen in simulations with an informative proxy. These results highlight but do not resolve the critical question of how best to use proxy information while minimizing the potential for proxy-induced error.

Keywords: Bayesian data fusion, Markov random field, numerical models, remote sensing, spatio-temporal modeling, splines

1 Introduction

There has been substantial interest recently in combining observations at spatial point locations with proxy information from remote sensing and numerical model output, particularly in the area of air quality. The goal is usually improved prediction of spatial and spatio-temporal surfaces. Building on Fuentes and Raftery (2005), statisticians have proposed a number of modeling approaches, often termed 'data fusion'. Most use Bayesian hierarchical spatial models to combine information sources with goals such as air quality management, forecasting, and exposure prediction for health analysis. Critically, model output and remote sensing retrievals often produce highly spatially-correlated surfaces, but some of this structure may represent spatially-correlated

error with regard to the quantity of interest. For example, a numerical model may overpredict a pollutant over a wide area because of shortcomings in information on emissions sources, while cloud or surface contamination may cause spatially-correlated errors in satellite retrievals. This 'error' is better termed discrepancy or offset when the proxy is not designed to estimate the focal process of interest but rather some related quantity.

In the statistical formulations of the problem, the possibility of proxy discrepancy has generally been acknowledged, but previous modeling efforts have often placed strong constraints on the structure of the discrepancy for reasons of identifiability or computational feasibility. Fuentes and Raftery (2005) proposed the following general model with their proxy (numerical model output) treated as data via a second likelihood,

$$\begin{aligned} Y_i &= L(\mathbf{s}_i) + \epsilon_i \\ A_j &= \phi(\mathbf{s}_j) + \beta_1(\mathbf{s}_j)L(\mathbf{s}_j) + e_j. \end{aligned} \tag{1}$$

The model relates both the gold-standard observations, Y_i , $i = 1, \dots, n$, and the proxy values, A_j , $j = 1, \dots, m$ (A for auxiliary), to the latent, true process of interest (the focal process), $L(\mathbf{s})$, at location \mathbf{s} . For the moment I suppress any change-of-support manipulations in defining $L(\mathbf{s}_j)$ when \mathbf{s}_j is an area. $\phi(\cdot)$ and $\beta_1(\cdot)$ are additive and multiplicative bias terms. In general it will be difficult to identify both $\phi(\cdot)$ and $\beta_1(\cdot)$, and Fuentes and Raftery (2005) use a scalar β_1 and take $\phi(\cdot)$ to be a simple polynomial in the spatial coordinates. Critically, since the additive bias has a very low dimensional representation, this approach assumes that all of the small- and moderate-scale spatial structure in the proxy is signal with respect to $L(\cdot)$. Paciorek and Liu (2009) used such a structure (1), with remote sensing retrievals playing the role of the proxy, but chose a reduced rank spline basis for additional flexibility in modeling the discrepancy. We found that model fitting was sensitive to the number of basis functions, with increasingly better fits as the number of basis functions increased, such that computational complexity prevented fitting a model with sufficiently many basis functions to model $\phi(\cdot)$ adequately. Other recent work has used such moderately flexible specifications for quantities analogous to $\phi(\cdot)$: Fuentes et al. (2008) used a small number of basis functions, while McMillan et al. (2010) used b-splines in two dimensions.

The dangers in limiting the flexibility of the discrepancy representation are that systematic discrepancies will bias prediction of the spatial process of interest in subdomains and that correlated uncertainty will not be properly acknowledged. In short, spatially-correlated discrepancy in the proxy may look like signal because of the dependence structure, but will cause spurious features in the prediction surfaces. Gold-standard data can help to assess the potential for discrepancy at scales resolved by the data. For large scales (relative to the data density), one can hope to estimate and adjust for the discrepancy. At smaller scales, one can at best hope to discount, but not adjust for, proxy information if the data indicate that the proxy is poorly related to the focal process. The key to this effort lies in using a sufficiently flexible model specification for the spatial discrepancy term.

I propose to represent the discrepancy, $\phi(\cdot)$, using a computationally efficient Markov random field (MRF) specification that is sufficiently flexible to model discrepancies at a variety of spatial scales. This MRF specification (Rue and Held, 2005; Yue and Speckman, 2010) approximates a thin plate spline while retaining the sparse precision matrix structure of more widely used MRFs, such as conditional autoregressive (CAR) models based on neighborhood adjacencies. For proxy variables that are often very high-dimensional (remote sensing and numerical model output on

large grids), modeling $\phi(\cdot)$ efficiently is critical. The ability of the proposed MRF specification to capture variation at a range of spatial scales stands in contrast to standard spatial representations: (1) Reduced rank basis function approaches (Kammann and Wand, 2003; Ruppert et al., 2003; Banerjee et al., 2008) can capture large-scale structure but require many knots with associated computational slowdowns for small-scale structure. (2) Traditional CAR models are computationally tractable and capture small-scale variability, but show small-scale variation when attempting to represent large-scale processes for which small-scale variability is absent.

The potential for improving prediction using data fusion is very appealing in applications. However, Paciorek and Liu (2009) found no improvement in fine particulate matter (PM) prediction using two satellite aerosol products, nor did McMillan et al. (2010) for PM prediction using output from the Community Multiscale Air Quality (CMAQ) atmospheric chemistry model. Sahu et al. (2009) found a statistically significant regression coefficient for the relationship between CMAQ output and their process of interest, but the magnitude of the coefficient was small, and there appears to be little evidence of predictive improvement from including the proxy. Berrocal et al. (2009) did find improvement in prediction of ozone relative to ordinary kriging without covariates when including the CMAQ proxy as a covariate. An important concern with regard to prediction in data fusion is that overly constrained discrepancy terms implicitly assume the proxy is useful and data fusion successful. Yet in analyses with constrained discrepancy, the change in the predictions from inclusion of the proxy may primarily reflect discrepancy rather than increased information.

My contribution is to present an approach that allows one to focus on these questions: is the proxy useful and data fusion successful; at what scales is the proxy useful and at what scales does it give erroneous predictions; and can one use the real information in the proxy and discount the influence of the discrepancy component? I propose a specific diagnostic for assessing the scales of discrepancy as a standard part of data fusion. My particular applied goal is to assess and, if helpful, use aerosol remote sensing retrievals and atmospheric chemistry model output to better predict spatial patterns in monthly average PM across the eastern United States, improving upon current spatio-temporal modeling efforts that combine smoothing with land use and meteorological covariates (Yanosky et al., 2009; Paciorek et al., 2009; Szpiro et al., 2009). I illustrate the methodology in the following related analyses: (1) spatial analysis of monthly PM in 2004 in the mid-Atlantic U.S. based on remotely-sensed aerosol optical depth (AOD), (2) spatio-temporal analysis of monthly PM in 2001 in the mid-Atlantic U.S. based on output from CMAQ, and (3) spatial analysis of monthly PM in 2001 in the eastern U.S. based on CMAQ output. I analyze the scales of the discrepancy and assess improvements in predictive performance from including the proxy.

2 Model and methods

In this section I outline the basic modeling approach, while technical details of the three specific models used in the examples and the Markov chain Monte Carlo (MCMC) fitting methods are provided in the Appendix.

2.1 Spatial latent variable model

I propose the following basic spatial model

$$\begin{aligned} Y_i &= \beta_y(x_{y,i}) + \mathbf{P}_{Y,i}\mathbf{L} + \epsilon_i \\ A_j &= \phi(s_j) + \beta_1\mathbf{P}_{A,j}\mathbf{L} + e_j \end{aligned} \quad (2)$$

where notation follows (1), with \mathbf{L} the vectorized representation of a spatial latent variable represented the process of interest on a fine base grid. $\beta_y(x_{y,i})$ is an regression function that represents sub-grid scale variability based on a single (for notational simplicity) covariate, while $\mathbf{P}_{Y,i}$ and $\mathbf{P}_{A,j}$ are rows of mapping matrices that pick off elements of \mathbf{L} to map to the observations and proxy values respectively. \mathbf{P}_A will generally also weight the focal process values to account for spatial misalignment of the proxy and base grids (particularly relevant for irregular remote sensing grids). By virtue of relating point level measurements to a grid-based latent process, the model has some of the flavor (and the computational advantages) of the measurement error model of Sahu et al. (2009), although $\beta_y(\cdot)$ allows for sub-grid heterogeneity. I take the error terms, ϵ_i and e_j , to be normally-distributed white noise.

I then represent $L(\mathbf{x}, \mathbf{s}) = \sum_p \beta_{L,p}(x_{L,p}) + g(\mathbf{s})$ as the sum of multiple regression terms, $\beta_{L,p}(x_{L,p})$, where $x_{L,p}$ is the p th covariate, and remaining spatial variation, $g(\mathbf{s})$. $\beta_y(\cdot)$ and $\beta_{L,p}(\cdot)$ may be simple linear terms or smooth regression terms to capture nonlinearity, in which case I use the mixed model formulation of a penalized thin plate spline (cubic radial basis functions in one dimension), where the unknown variance component of the exchangeable basis coefficients controls the amount of smoothing (Ruppert et al., 2003; Crainiceanu et al., 2005). When the covariates are able to represent most of the small-scale variation in the focal process, $g(\cdot)$ need only explain large-scale variation, so one approach is represent $g(\cdot)$ using a penalized thin plate spline, as I do for the analyses in the mid-Atlantic region (Sections 4.1-4.2). Alternatively, when the knot-based representation of $g(\cdot)$ requires so many knots that computations bog down, either because of small-scale process variation or a large domain, $g(\cdot)$ can be represented as a MRF, as described next for $\phi(\cdot)$ and used in the analysis of CMAQ output in the eastern U.S. (Section 4.3).

For $\phi(\cdot)$, I use the MRF approximation of a thin plate spline, $\phi \sim \mathcal{N}_{m-3}(0, (\kappa\mathbf{Q})^-)$, described in detail in Section 2.2. \mathbf{Q} is the MRF weight matrix, with rank $m - 3$, hence the use of the generalized inverse, while κ is a precision parameter. This approach allows the discrepancy to represent either smooth large-scale variation or wiggly small-scale variation depending on the data, while providing computational feasibility. I work with up to $m = 17,500$ pixels in the analyses. Note that integrating over ϕ produces a spatially-correlated proxy covariance structure.

2.2 Markov random field specification

MRF models often use simple binary weights in which direct neighbors are given a weight of one and all other locations are given zero weight (e.g., standard CAR models). However, such models have realizations with unappealing properties. Rue and Held (2005) characterize the intrinsic Gaussian CAR model in one dimension as a discretely observed Wiener process (i.e., one-dimensional Brownian motion), while Besag and Mondal (2005) show that the intrinsic Gaussian CAR model on a fine two-dimensional grid approaches two-dimensional Brownian motion (the de Wijs process) asymptotically as the grid resolution increases. Brownian motion has continuous but not differentiable sample paths, so it is not surprising that the process realizations of standard CAR

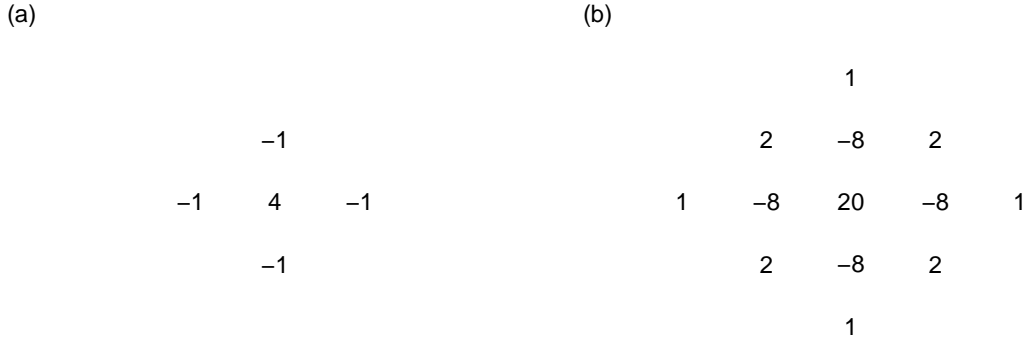


Figure 1: Neighborhood structure and weight matrix elements for a single row of the weight matrix, \mathbf{Q} , with the non-zero elements represented spatially relative to the focal grid cell (a non-boundary cell) for (a) a standard MRF model with binary weights, with weight only on the nearest neighbors in the cardinal directions compared to (b) an MRF model with weights based on the thin plate spline approximation.

models are locally heterogeneous, as seen next, regardless of the value of the variance component for the process.

A more flexible alternative that has received little attention but is potentially widely-applicable is an intrinsic Gaussian MRF whose weight structure is motivated by the smoothness penalty that induces the thin plate spline (henceforth a TPS-MRF) Rue and Held (2005); Yue and Speckman (2010). For a regular grid, Fig. 1 compares the neighborhood and weight structure of the standard CAR model with binary weights to that for the TPS-MRF. Note that the presence of both positive and negative values in the precision matrix bears similarity to the oscillations and negative values in the equivalent kernels for spline smoothing and Gaussian process smoothing (Silverman, 1984; Sollich and Williams, 2005). In the Appendix, I show the full set of values that define the weight matrix, \mathbf{Q} , for the TPS-MRF, including the boundary effects. Fig. 2 shows the fitted posterior mean surface under the standard CAR and TPS-MRF models for a simulated dataset whose true surface is very smooth; note the local heterogeneity induced by using the CAR model. To demonstrate the need for smooth process specifications for proxy error, consider the smooth, albeit gridded, variation in the CMAQ output in Fig. 7).

2.3 Spatio-temporal latent variable model

For a spatio-temporal extension to the model, I allow \mathbf{g}_t , $t = 1, \dots, T$, to vary smoothly in time with a common mean and autoregressive temporal dependence, while I treat ϕ_t exchangeably with a common mean capturing overall spatial variation. The inclusion of a common mean is a general principle that allows for appropriate estimation of uncertainty in long-term averages (Stein and Fang, 1997).

Using the mixed model representation of $g(\cdot)$ as a penalized thin plate spline on the latent process grid, $\mathbf{g} = \mathbf{Z}_g \mathbf{b}_g$, $\mathbf{b}_g \sim \mathcal{N}_K(\mathbf{0}, \sigma_{b_g}^2 \mathbf{I})$ (Ruppert et al., 2003; Crainiceanu et al., 2005), I use an autoregressive model for the temporally-varying coefficients for each spatial knot, $\mathbf{b}_{g,k} \sim$

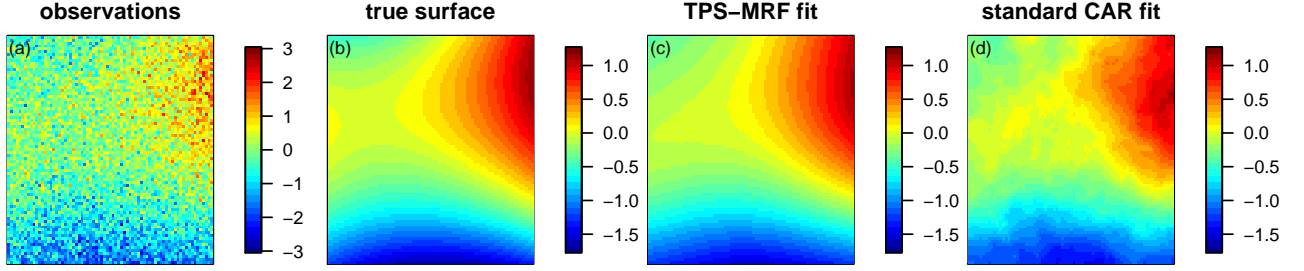


Figure 2: For simulated data (a) based on white noise added to a smooth true surface (b), (c) shows the posterior mean under the TPS-MRF model and (d) the posterior mean under a MRF model with a standard CAR neighborhood structure.

$\mathcal{N}_T(u_k \mathbf{1}, (1-q)\sigma_{b_g}^2 \mathbf{R}(\rho))$, $k = 1, \dots, K$. I marginalize over a mean parameter for each knot, with the means exchangeable across knots, $u_k \stackrel{iid}{\sim} \mathcal{N}_K(0, q\sigma_{b_g}^2 I)$. This gives the representation $\mathbf{b}_{g,k} \sim \mathcal{N}_T(\mathbf{0}, \sigma_{b_g}^2 (q\mathbf{J} + (1-q)\mathbf{R}(\rho_g)))$ where \mathbf{J} is a matrix of ones, $\mathbf{R}(\rho_g)$ is an AR(1) autocorrelation matrix, parameterized by decay parameter ρ_g , and $q \in (0, 1)$ weights the exchangeable and autocorrelated contributions to the variance. Considering all the coefficients across times and knots jointly I have $\mathbf{g} = \{\mathbf{g}_1, \dots, \mathbf{g}_T\} = \mathbf{Z}_g^* \mathbf{b}_g^*$ where \mathbf{Z}_g^* is blocked.

For the temporal structure of the discrepancy, one simple approach is to specify an exchangeable structure,

$$\begin{aligned} \phi_t &\sim \mathcal{N}_{m-3}(\phi_{\text{mean}}, (\kappa_1 \mathbf{Q})^-) \\ \phi_{\text{mean}} &\sim \mathcal{N}_{m-3}(\mathbf{0}, (\kappa_2 \mathbf{Q})^-) \end{aligned}$$

and marginalize over the common mean to derive an improper joint prior, $\phi = \{\phi_1, \dots, \phi_T\} \sim \mathcal{N}_{(m-3)T}(\mathbf{0}, (\mathbf{D}(\kappa_1, \kappa_2) \otimes \mathbf{Q})^-)$, for the discrepancy terms for all the months combined, where \mathbf{D}^{-1} is a T by T matrix with diagonal elements, $\frac{1}{\kappa_1} + \frac{1}{\kappa_2}$, and off-diagonal elements, $\frac{1}{\kappa_2}$. One could specify an AR(1) structure in addition to a common mean, which gives an improper prior with similar structure, with \mathbf{D}^{-1} having diagonal elements, $\frac{1}{(1-\rho_\phi^2)\kappa_1} + \frac{1}{\kappa_2}$, and off-diagonals,

$$D_{ij}^{-1} = \left(\frac{\rho_\phi^{|i-j|}}{(1-\rho_\phi^2)\kappa_1} + \frac{1}{\kappa_2} \right), \text{ where } \rho_\phi \text{ is the correlation parameter.}$$

2.4 Modeling scenarios and the spatial scales of discrepancy

2.4.1 Discrepancy scenarios

One important goal in including the spatial discrepancy term is to understand the scales at which the proxy and the process of interest are well- and poorly-correlated. I posit a range of potential relationships. These represent extreme scenarios, so in any practical problem the reality is likely a combination of scenarios.

- Scenario A (white noise discrepancy): the spatial structure in the proxy mirrors that in the focal process but there is fine-scale discrepancy at the scale of pixels that can be treated

as white noise. Under this scenario there is no need for $\phi(\cdot)$ given the white noise error structure, $\{e_j\}$. Smoothing over the proxy gives information about the process of interest.

- Scenario B (small-scale discrepancy): the proxy accurately reflects the focal process at large scales, but there is smaller-scale correlated discrepancy. Under this scenario, models without a sufficiently flexible discrepancy term may treat the discrepancy as signal since it is not white noise. Or, if the discrepancy is large enough in magnitude, one would expect the estimate of β_1 to be attenuated, hindering use of the large-scale information in the proxy. In contrast, with a flexible representation of $\phi(\cdot)$, the model can treat the discrepancy as having small-scale spatial dependence, thereby ignoring this component of variation in the proxy. Note that without dense data, the model cannot correct for the small-scale discrepancy. Also, unless there are large spatial gaps in the observations, it's not clear if using the proxy to help estimate large-scale variation will improve upon simply smoothing the gold standard data.
- Scenario C (large-scale discrepancy): the proxy accurately reflects small-scale variation in the focal process, but there is large-scale discrepancy. In this case, one can correct for this large-scale mismatch through estimation of $\phi(\cdot)$ (needing only moderate amounts of gold standard data) and predict small-scale variation in the focal process from small-scale variation in the proxy. This scenario is accommodated by other approaches in the data fusion literature that constrain the discrepancy to vary only at larger spatial scales.
- Scenario D (uninformative proxy): the proxy and focal process are at best weakly related at all scales and β_1 is near zero. In this case a model without a flexible discrepancy term may have trouble representing the proxy reasonably. Without a flexible discrepancy term, if there are limited gold standard data the focal process prediction may be driven largely by the proxy and β_1 may be estimated to be far from zero. This allows the variation in the proxy to be explained by a spatial process rather than by white noise (with higher accompanying posterior density, analogous to a penalized likelihood setting), even at the expense of increasing the error variance for the observations.

Note that when $\phi(\cdot)$ is estimated as a large-scale process it is analogous to including spatial variation in the mean, and one might think of this as correcting for spatial bias. When $\phi(\cdot)$ is estimated as a small-scale process, it is analogous to accounting for spatial variation through the variance term, with a short spatial range. Given the equivalence between a stochastic process in the mean and integrating over that process to move the variation into the covariance, I believe the distinction between representation in the mean and variance is artificial and instead focus on understanding the scale of the discrepancy. In all cases, within a given subdomain, one can think of the discrepancy as causing local bias in the predicted surface if treated as signal.

2.4.2 Spatial discrepancy diagnostic

To assess the spatial scales of the discrepancy term, I propose to use a spatial variogram-based diagnostic introduced by Jun and Stein (2004) for assessing numerical model performance relative to observations. They calculate variograms for the model output, observations, and model error (defined as model output minus observations). They propose the ratio of the model error variogram to the sums of the variograms for model output and observations as a distance-varying diagnostic

of the spatial variation in the observations captured by the model output. If the model output and observations were independent, then the variogram of the error would be the sum of the variograms of output and observations, so the ratio would be one on average. My analog plugs the analogous quantities from the statistical model (2) into their diagnostic, using $\beta_1 \mathbf{L}$ as the best estimate of the focal process, scaled to the units of the proxy:

$$M(d) = \frac{\text{Variog}(\phi; d)}{\text{Variog}(\phi + \beta_1 \mathbf{L}; d) + \text{Variog}(\beta_1 \mathbf{L}; d)}.$$

The interpretation is the proportion of the variation in the proxy that is accounted for by the discrepancy term, as a function of spatial scale, quantified by distance, d . The diagnostic has the following appealing extremal properties: when $\beta_1 = 0$ or if ϕ offsets all the variation in the focal process at a given scale, $M(d) = 1$, indicating all of the variability in the proxy is explained by discrepancy. In the ideal situation when $\phi = 0$ in general or has no variation at a given scale, then $M(d) = 0$, indicating all of the variability in the proxy at the scale is explained by the process of interest.

2.5 Marginalization and MCMC sampling

The proposed modeling approach contains two spatial or spatio-temporal latent processes that can trade off in explaining variation in the proxy. In addition there is cross-level dependence between the latent process values and the hyperparameters controlling spatial and spatio-temporal process dependence and variation. This raises concerns about MCMC convergence and mixing if the processes are proposed separately or a process and its hyperparameters are proposed separately. Poor mixing in such situations is common, and marginalization over the process or joint sampling of a process and its hyperparameters (Rue and Held, 2005; Paciorek, 2007) are often used, when possible, to improve mixing. Here the high-dimensionality of the processes complicates matters further. The modeling approach allows for marginalization over the process values and then efficient computations based on sparse matrix manipulations, described briefly here and in more detail in the Appendix.

In particular, for the spatial model, I marginalize first over the MRF, ϕ , and then over the basis coefficients for the regression terms to produce a representation of the marginal posterior for which I can use sparse matrix manipulations when sampling the remaining parameters by the Metropolis algorithm. When the focal process is represented as a reduced rank thin plate spline, its process values are part of this second marginalization over the basis coefficients and when the focal process is also represented as an MRF, I marginalize over it in conjunction with ϕ . In the spatio-temporal model, the assumptions about the dependence structure of the discrepancy allow one to first marginalize over it and then over the basis functions to again allow for sparse matrix computations in sampling the remaining parameters. Note that even with these efforts, sampling can be slow; for the space-only models for the mid-Atlantic run times are on the order of 6 hours, while for the space-only eastern U.S. models and space-time mid-Atlantic models, run times are on the order of 3-5 days. Much of this is required to achieve good mixing of the variance components for the MRF and spline basis coefficients without the use of informative priors.

3 Simulations

3.1 Methods

To assess the performance of the approach, including the decomposition of proxy variability between the discrepancy term and focal process, I fit a simplified version of the spatial model to simulated data under a variety of scenarios:

1. Large- and small-scale discrepancy present with $\beta_1 = 1$
2. Large- and small-scale discrepancy with $\beta_1 = 0$
3. No spatial discrepancy, $\beta_1 = 1$
4. Large-scale discrepancy only, $\beta_1 = 1$
5. Small-scale discrepancy only, $\beta_1 = 1$
6. Sparse observations ($n = 40$), with some small-scale discrepancy and a minor amount of large-scale discrepancy, $\beta_1 = 1$

The data were simulated based on the setting of the monthly mid-Atlantic analyses, with similar number of gold-standard observations, $n = 171$ (except for scenario 6). I simulated and fit with linear effects of a small number of land use covariates, with those covariates taking the same values as in the mid-Atlantic domain, but with some of the covariates transformed differently in the data generation than in the fitting process, as well as simulated residual spatial surfaces, \mathbf{g} , operating at two different scales, and simulated discrepancy, ϕ at the scales indicated above, all based on Gaussian process realizations (with range parameters chosen to achieve the desired scale of variability). Note that the surface generation model differs from the MRF spatial process representation in the model. The proxy is fully-observed over the entire 175x100 grid with no misalignment and with white noise discrepancy in all cases, but I calculate the likelihood only for land-based pixels. The white noise components of the error structures for the observations and proxy are simple homoscedastic normal error structure, with multiple observations within a grid cell are modeled as described in the Appendix.

3.2 Results

In general, the model is able to predict spatial variation in the true process reasonably well in these settings, but it does not exploit the information the proxy effectively. Predictive performance generally decreased when including the proxy compared to fixing $\beta_1 = 0$, with the R^2 decreasing from 0.81 when ignoring the proxy to between 0.70 and 0.72 when including it in scenarios 1, 4, and 5. In scenario 2, the model correctly estimates that $\beta_1 \approx 0$ and does not lose any predictive power. In scenario 3, the R^2 also decreases, to 0.70, with the model attributing some of the signal to the discrepancy term.

This suggests that the added information in the proxy is offset by the model's inability to sufficiently screen out discrepancy in the proxy. Except in scenario 2, including the proxy as a regressor, rather than a second likelihood, does improve prediction (to R^2 values of 0.84, 0.82, 0.90,

0.87, and 0.83 in the first five scenarios respectively). Assuming $\phi = 0$ or that ϕ can be represented as very smoothly varying in space in general leads to much worse predictive performance, except in scenario 3, for which R^2 is 0.91 with ϕ excluded and 0.95 with ϕ represented smoothly. The one case where the full model outperforms a model that ignores the proxy is scenario 6, for which the R^2 is 0.34 in the full model and less than 0 in the model without the proxy (i.e., the sum of squared errors is larger than the empirical variation in the true focal process values). In scenario 6, using the proxy as a regressor again performs better than the two likelihood approach, with $R^2 = 0.49$. In all scenarios, the estimated β_1 in the full model and estimated regression coefficient for the proxy when it is used as a regression term are attenuated relative to the true value of 1. Finally, the estimated discrepancy surfaces reasonably match the true discrepancy (not shown). I conclude that not including the discrepancy term is dangerous when discrepancy is present, but that the proposed model is not able to exploit the signal present in the proxy to improve prediction when the gold standard data are relatively dense.

Fig. 3 shows the discrepancy scale diagnostic (Section 2.4.2) for the full model under each scenario. In general, there appears to be some, but imperfect, information in the diagnostic about the scale of discrepancy, with the expected relationship with scale given the data generation for a given scenario. That is, when there is more discrepancy at large than small scales the ratio should increase with distance and when there is more discrepancy at small than large scales, it should decrease. However, even when there is no true discrepancy at a scale the diagnostic estimates discrepancy, which is caused by the attenuated estimates of β_1 , suggesting that one should treat the diagnostic as indicative, rather than conclusive, about the scales of discrepancy. Also, the diagnostic results suggest caution in interpreting the diagnostic at the shortest distances, given the drop in the diagnostic even for the scenarios with small scale discrepancy (scenarios 1, 5, and 6).

4 Examples

I modeled fine PM (also called $\text{PM}_{2.5}$) in the eastern U.S. and assessed the use of remote sensing AOD retrievals and CMAQ output as proxies. In the first analysis (Section 4.1) I fit separate spatial models for each month of 2004 for the mid-Atlantic region with AOD from the MODIS instrument as the proxy. In contrast with previous work on this domain (Paciorek and Liu, 2009), where I used a knot-based thin plate spline for $\phi(\cdot)$ and found that the estimated discrepancy was estimated to be increasingly wiggly as more knots were added until fitting became too computationally intensive, here I use the TPS-MRF for $\phi(\cdot)$. Next, in Section 4.2, I considered instead CMAQ output in the mid-Atlantic as a proxy and jointly fit all 12 months of 2001 (full CMAQ output was only available to me for this year) with the spatio-temporal model. Given the lack of relationship between the remote sensing retrievals and the latent seen in the separate monthly spatial analyses (Section 4.1) and the much greater computational burden for the 17500 AOD grid cells compared to the CMAQ grid cells, I did not carry out a full spatio-temporal analysis for the remote sensing data. Finally, in the third analysis (Section 4.3), I fit separate monthly spatial models for 2001 for the entire eastern U.S. to assess the CMAQ proxy at larger scales and better understand the scale decomposition and discrepancy term. One issue with the first two analyses is that some PM monitors do not report every day (reporting every third or sixth day), which increases the noise in the PM monthly averages. To avoid any temporal misalignment, I restricted the third analysis to monthly averages of PM data and CMAQ output from every third day and used only ground monitors reporting

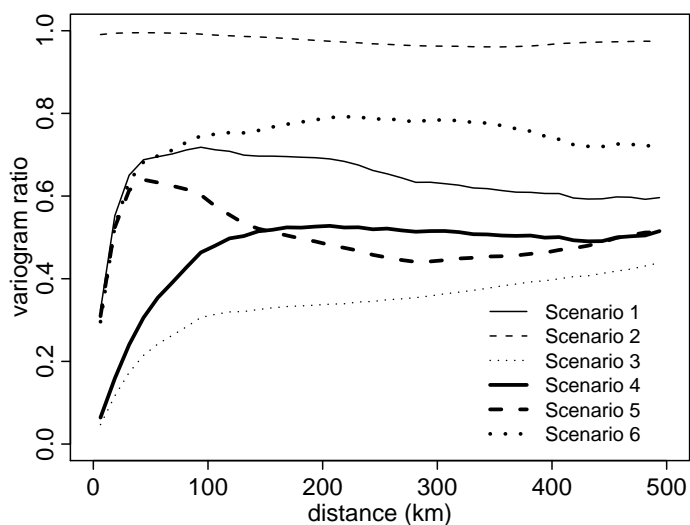


Figure 3: Discrepancy scale diagnostic for the model fit to simulated data under various scenarios: (1) large- plus small-scale discrepancy (thin line), (2) uninformative proxy (thin dashed line), (3) no spatial discrepancy (thin dotted line), (4) large-scale discrepancy only (thick line), (5) small-scale discrepancy only (thick dashed line), and (6) sparse data with some small-scale and minor large-scale discrepancy (thick dotted line).

every day or every third day. Full details on the various data sources and data pre-processing manipulations are provided in our peer-reviewed Health Effects Institute research report (Paciorek and Liu, submitted).

The observations are monthly averages of available 24-h PM concentrations from the U.S. EPA Air Quality System. For simplicity and because I use monthly averages, I do not transform the PM values, in contrast to other work on PM (Smith et al., 2003; Yanosky et al., 2009), but log or square root transformations are good alternatives. For regression terms that represent sources, additivity on the original scale makes more sense while for modifying variables such as meteorology, log transformation to scale multiplicatively makes more sense. Achieving both in a single model is not easily accomplished. I note that the long right tail of CMAQ output may be accommodated through ϕ because the CMAQ output is spatially correlated. As in Paciorek et al. (2009), residuals from the various models indicated long-tailed behavior, reasonably characterized by t distributions with approximately 5 degrees of freedom, albeit with right skew. Predictive performance suggests that the influence of outliers is not extreme, but the use of a t distribution for the observation errors would be worth exploring. However, this would be somewhat difficult to do in the context of the additive error structure I derive based on components of variability in the PM measurements (see Appendix).

In the next subsections, I outline the basic models and highlight results. I also show plots that illustrate the estimated spatial structure of PM and of the discrepancy, and the proposed discrepancy scale diagnostic. I report nine-fold cross-validation prediction results. I have retained a tenth set to assess the degree of overfitting that may have been caused through the model selection process (Draper and Krnjacic, 2006), saving this set for our ongoing work.

Table 1: Simple correlations of observations and proxy values (all available values, not matched by day) with the proxy values based on the pixels in which PM observations fall.

Time scale	mid-Atlantic, 2004, MODIS AOD	mid-Atlantic, 2001, CMAQ	eastern U.S., 2001, CMAQ
Monthly ¹	0.58 (0.60 uncalibrated)	0.26	0.52
Yearly ²	0.60 (0.26 uncalibrated)	0.095	0.56

¹ Including only monthly averages based on at least five daily observations.

² Including only yearly averages based on at least nine months with at least five daily observations, with yearly averages calculated as the mean of the 12 monthly averages.

For context, in Table 1, I show raw correlations at the monthly and yearly aggregations between the raw observations and the proxy variables. MODIS AOD is moderately correlated with the observations, while CMAQ in the mid-Atlantic region is poorly correlated and CMAQ in the eastern U.S. moderately correlated with the observations.

4.1 Spatial analysis of MODIS AOD in the mid-Atlantic region

Here I used AOD from the MODIS instrument, which at each orbit provides a snapshots of a swath of the eastern U.S. at approximately 10:30 am, generally giving a value for any fixed location every 1-2 days. AOD is a dimensionless measure of light extinction through the entire vertical column of the atmosphere, which is generally correlated with PM at the ground surface. MODIS AOD is estimated by an algorithm based on light sensed by the satellite instrument and is available on an irregular grid with an approximate resolution of 10 km. For this analysis, I used a regular four km grid of dimension 175 by 100 as the resolution of $L(\cdot)$, $g(\cdot)$, and $\phi(\cdot)$. MODIS AOD is misaligned with respect to this grid and for different satellite orbits on different days, the pixels shift spatially. Therefore, I considered the overlap of all the pixels in an orbit with the four km grid, assigning to each grid cell, s_j , the value of the MODIS pixel in which the cell centroid falls. Taking the retrievals assigned to each cell, I then averaged to the monthly level for each cell. More sophisticated approaches are possible (Mugglin et al., 2000), but for these purposes, this ad hoc realignment retained the essential character of the AOD retrievals and reduced computations. I attempted to account in part for informatively missing AOD due to cloud cover (Paciorek et al., 2008) by including a smooth regression term $\beta_a(x_a)$ in the additive mean for the proxy, thereby making a missing-at-random assumption. x_a is the average cloud cover over the month for each location (using the cloud screen variable from the Geostationary Operational Environmental Satellite. $g(\cdot)$ is modeled using the thin plate spline mixed model representation. Distance to nearby roads in two road size classes, calculated for each monitor location, were used as smooth spline terms, $\beta_{y,p}(x_{y,p})$, $p = 1, 2$, while elevation, population density, road density in three road size classes, and area emissions were estimated at the four km resolution using a Geographic Information System and used as smooth spline terms, $\beta_{L,p}(x_{L,p})$, $p = 1, \dots, 6$. Distance to point source emissions (those greater than five tons per year) was handled as smooth function of distance, adding over the sources within 100 km of the observation (or grid cell), following the methodology of Paciorek and Liu (submitted, Appendix). I did not use meteorological covariates (obtained from the North American Regional Reanalysis (NARR) data product) as these proved to have high concurvity with the estimated residual spatial variation, g . This concurvity is driven by the fact that the covariates

vary primarily at large scales, presumably caused in part by the coarse 32 km resolution of the NARR grid.

I considered both raw MODIS AOD and a 'calibrated' MODIS AOD that adjusts off-line for the effects of boundary layer height and relative humidity, as well as large-scale temporal and spatial adjustments, based on comparison of co-located daily PM and AOD values (Paciorek and Liu, 2009).

The estimated regression coefficients for the latent PM as an explanatory variable for the proxy were essentially zero (Fig. 4e), indicating that the model found no relationship between the proxy and the estimated latent process, discounting the proxy in predicting PM. The spatial discrepancy plot indicates that at all scales the proxy is explained by the discrepancy term rather than the latent process at all scales (Fig. 4a). These results are consistent with those found in Paciorek and Liu (2009). Fig. 5 shows predictions from the model when excluding and including AOD, with very similar predictions, consistent with the estimated values of β_1 near zero. Given this, it is not surprising that the cross-validated predictive assessment indicated that including the proxy did not improve predictive performance (Table 2). (Yearly prediction appeared slightly worse when excluding the proxy, but this is likely within the uncertainty of the predictive assessment, which is difficult to quantify given the correlation structure of the data). Results were qualitatively similar when considering only held-out monitors in more rural areas, suggesting that AOD is not adding information in areas far from monitors (Table 2).

4.2 Spatio-temporal analysis of CMAQ output in the mid-Atlantic region

For this analysis, the spatial domain, covariates, and general model framework were as in the MODIS AOD analysis, but I used the 12 months of 2001, the year for which CMAQ output was available to me. CMAQ is a numerical atmospheric chemistry model that uses estimated meteorological fields and emissions sources as inputs and provides hourly estimates of PM and other atmospheric constituents in space and vertically through the atmosphere. I used the CMAQ 36 km square grid over the domain as the grid resolution of $\phi(\cdot)$ (dimension 19 by 11), relating L to the proxy on that grid with a mapping matrix P_A that calculates a weighted average of the latent process values in the four km cells falling in each 36 km CMAQ pixel. The CMAQ proxy was the average of predicted PM in each grid cell for the lowest vertical level of the model. I used the spatio-temporal formulation of Section 2.3 to build temporal dependence amongst the months for the $g_t(\cdot)$ surfaces and exchangeable dependence amongst the months for the $\phi_t(\cdot)$ surfaces. The assumption of exchangeability but no autocorrelation was supported by posterior assessment of the fitted $\phi_t(\cdot)$ surfaces. I specified a priori independent regression parameters for each month, $\beta_{1,t}$. Given the sensitivity to the temporal dependence structure reported below, I also fit simple monthly spatial models in the style of Section 4.1 but otherwise retaining the features discussed above. In the spatio-temporal analysis, in addition to the temporally-invariant covariates considered in Section 4.1, I also considered NARR-based meteorological covariates for L but found that they did not improve prediction.

For both the spatio-temporal formulation and the individual spatial models fit separately to each month, the estimated values of β_1 were larger in winter than summer (Fig. 4f). The discrepancy scale diagnostic plot suggests that more of the variation in the proxy at small scales is related to the latent process than at large scales (Fig. 4b). This likely relates to CMAQ correctly placing hot spots around the urban areas (Fig. 6). However, the model-estimated discrepancy surfaces indicate the

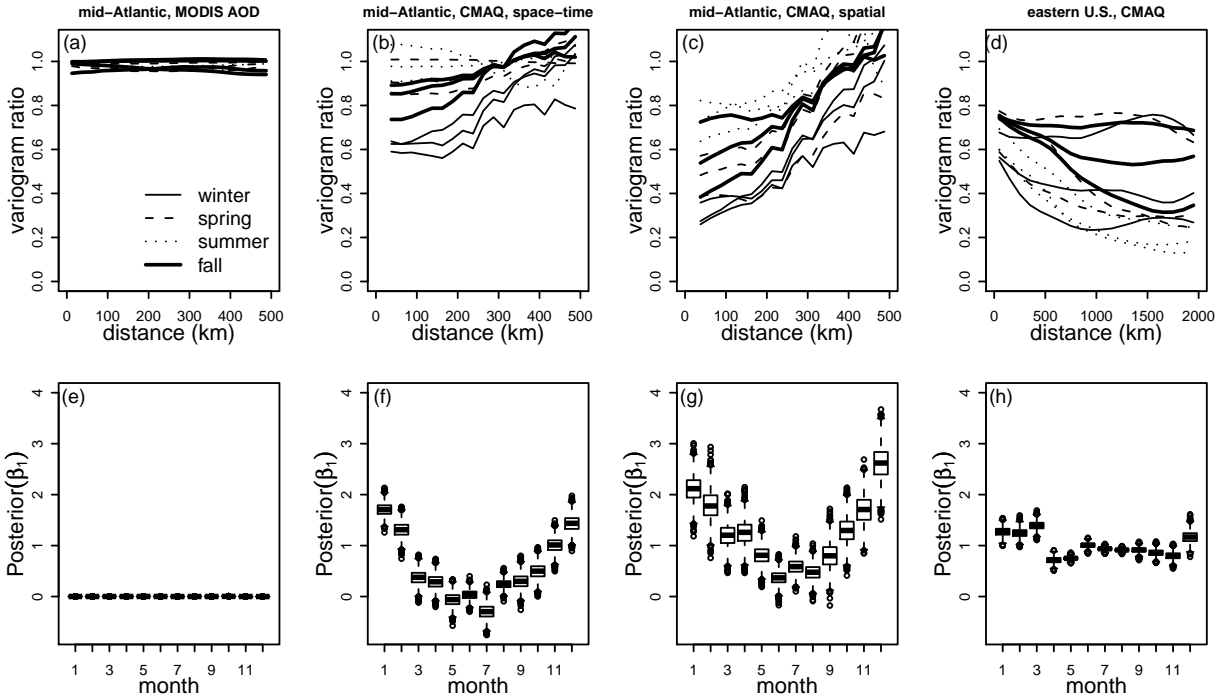


Figure 4: Discrepancy scale diagnostic plots (top row) and boxplots of posterior estimates of β_1 (bottom row) by month for analysis of MODIS AOD as the proxy in 2004 in the mid-Atlantic using the spatial model (far left panels), CMAQ as the proxy in 2001 in the mid-Atlantic using the spatio-temporal model (middle left), CMAQ as the proxy in 2001 in the mid-Atlantic using the spatial model (middle right), and CMAQ as the proxy in 2001 in the eastern U.S. using the spatial model (far right).

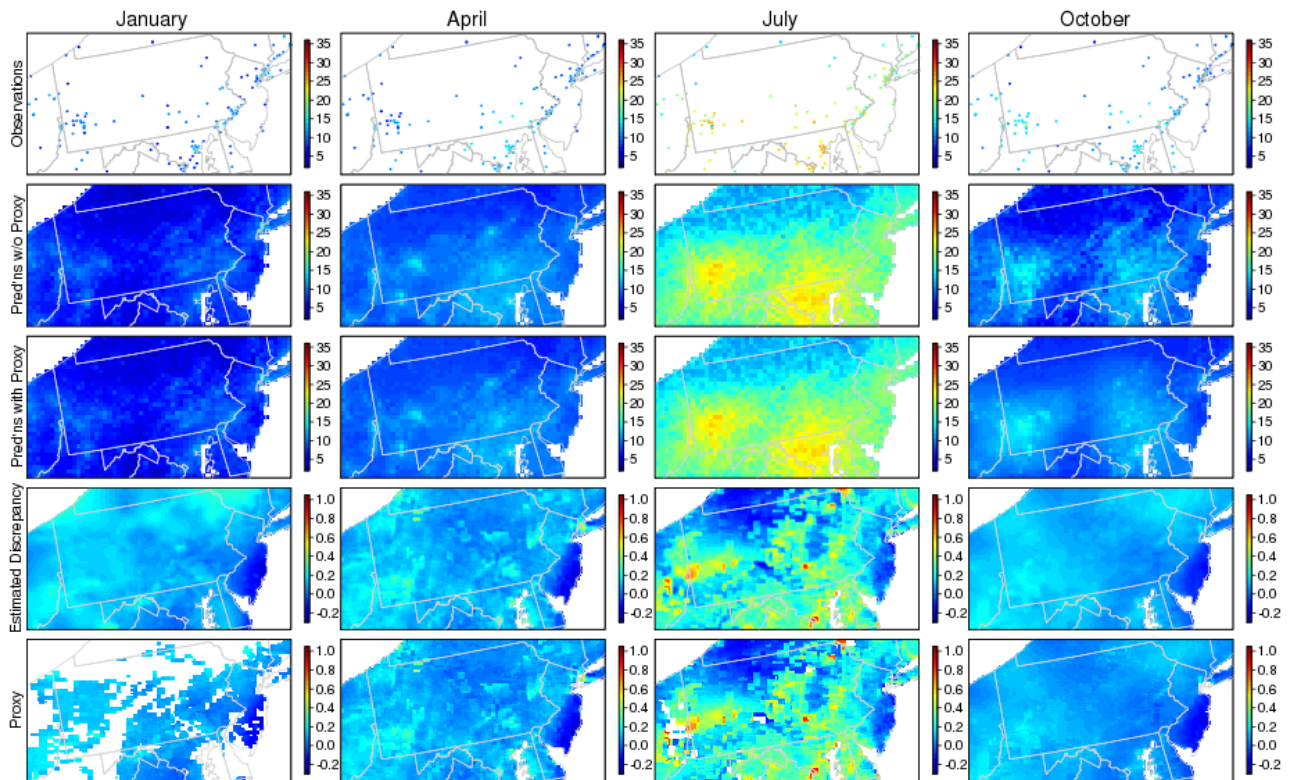


Figure 5: For the mid-Atlantic region of the U.S., PM observations (first row), model PM predictions excluding MODIS AOD (second row), model predictions including AOD (third row), estimated discrepancy in the model with AOD (fourth row), and AOD values (fifth row) for four months in 2004: January, April, July, and October (columns). White space in the land areas in the fifth row indicate AOD values missing because of cloud cover for all AOD retrievals in the month.

Table 2: Cross-validation predictive ability, R^2 (RMSPE), for monthly and yearly (average of the 12 monthly values) predictions, with and without proxy information, over the spatio-temporal domains of the three analyses.

Time scale	Proxy inclusion	mid-Atlantic, 2004, MODIS AOD	mid-Atlantic, 2001, CMAQ, spatio-temporal model	mid-Atlantic, 2001, CMAQ, spatial models	eastern U.S., 2001, CMAQ
All monitors					
Monthly prediction ¹	With proxy	0.806 (1.80)	0.640 (2.60)	0.755 (2.14)	0.827 (1.71)
	Without proxy	0.808 (1.79)	0.686 (2.42)	0.777 (2.04)	0.826 (1.72)
Yearly prediction ²	With proxy	0.667 (1.00) ³	< 0 ⁴ (1.97) ³	0.503 (1.32) ³	0.800 (1.21)
	Without proxy	0.650 (1.03) ³	0.169 (1.70) ³	0.584 (1.20) ³	0.835 (1.09)
Monitors generally isolated from other monitors ⁴					
Monthly prediction ¹	With proxy	0.830 (1.73)	0.626 (2.74)	0.721 (2.36)	0.739 (2.12)
	Without proxy	0.830 (1.72)	0.588 (2.87)	0.761 (2.19)	0.781 (1.94)
Yearly prediction ²	With proxy	0.669 (1.17)	< 0 ⁶ (1.99)	0.254 (1.67)	0.710 (1.58)
	Without proxy	0.624 (1.25)	< 0 ⁶ (1.94)	0.395 (1.51)	0.826 (1.22)

¹ Including monthly averages based on at least five daily observations. ²Including yearly averages (averages of monthly values) based on at least nine months with at least five daily observations. ³ Excludes one site outside Pittsburgh just downwind of a major industrial facility. ⁴Squared correlation of held-out data and predictions is 0.473, but observations vs. predictions are not centered on the one to one line, so error sum of squares exceeds total sum of squares. ⁵ Monitors in four km grid cells with fewer than 187.5 people per square km=3000 people per cell. ⁶ Observations vs. predictions are not centered on the one to one line, so error sum of squares exceed total sum of squares.

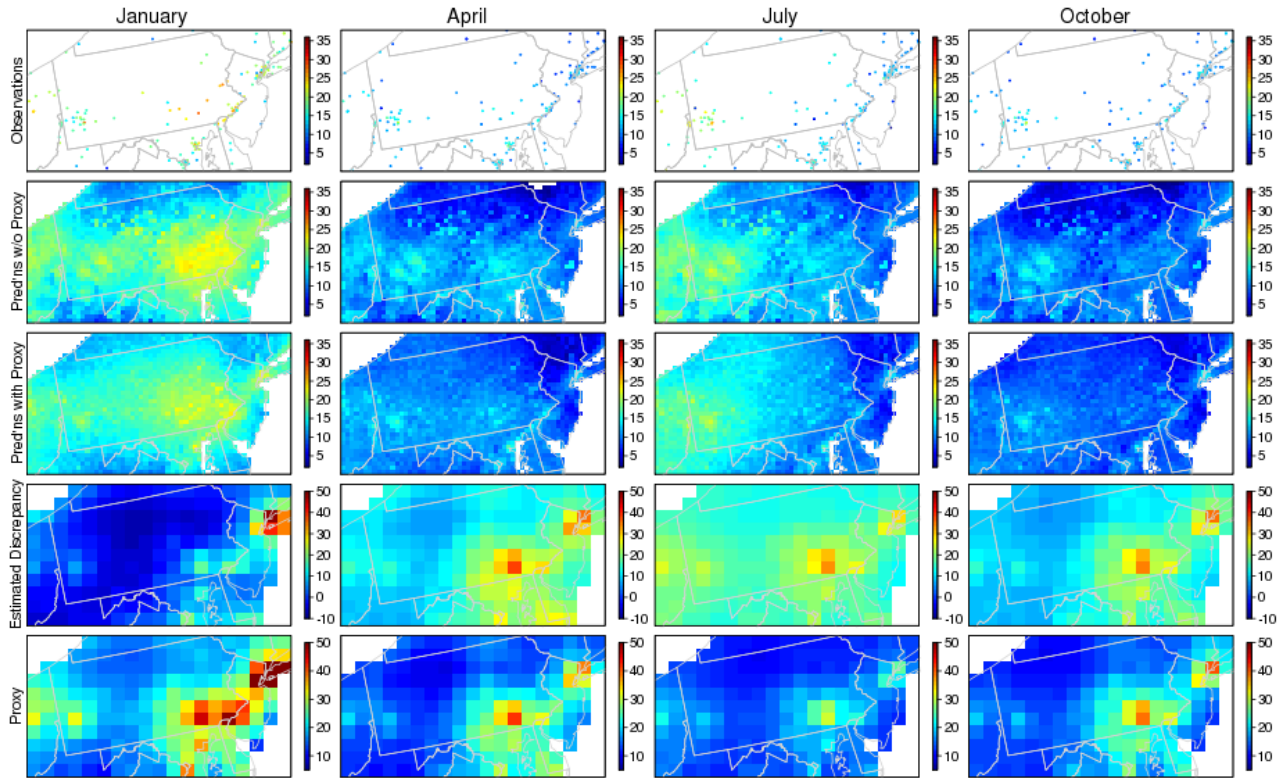


Figure 6: PM observations (first row), spatio-temporal model PM predictions excluding CMAQ (second row), model predictions including CMAQ (third row), estimated discrepancy in the model with CMAQ (fourth row), and CMAQ values (fifth row) for four months in 2001: January, April, July, and October (columns). Note that in January, some CMAQ values in the New York City area (which are as high as $75 \mu\text{g}/\text{m}^3$) are truncated to $50 \mu\text{g}/\text{m}^3$.

need to substantially correct the CMAQ output at larger scales and discount the CMAQ-estimated hotspot in southeastern Pennsylvania and moderate the hotspot over New York City, as these are not supported in the observations (Fig. 6). Fig. 6 also illustrates that CMAQ-estimated PM shows similar spatial patterns from month to month (represented in the exchangeable structure for the monthly discrepancy processes). This consistency over time contrasts with the spatio-temporal heterogeneity seen in raw observations, which suggests that CMAQ is not adequately capturing changing spatial patterns over time. For both models cross-validators predictive performance was as good or better when excluding the proxy compared to including the proxy (Table 2).

The spatio-temporal model predicted less well than simple spatial models for this domain, particularly for the yearly averages, even when the proxy is excluded (Table 2). Apparently forcing the same covariate relationships for all months and by smoothing and shrinking the spatial residual terms, $g_t(\cdot)$, reduced predictive performance. More investigation is warranted to better understand why smoothing over time did not help with predictive performance, but presumably relates to model misspecifications in the more complicated spatio-temporal model that do not match the structure of the data.

4.3 Spatial analysis of CMAQ output in the eastern United States

For this analysis, I extended the four km grid over the the eastern U.S. (roughly the area east of 100° W longitude), giving a grid of dimension 669 by 677. I used the 36 km CMAQ grid of dimension 73 by 77 for $\phi(\cdot)$. For this larger domain with more complexity in the pollution surface, I represented $g(\cdot)$ on this same 36 km grid using the TPS-MRF representation rather than the mixed model thin plate spline. The latter would have required a computationally burdensome increase in the number of basis coefficients. Note that I relied on the covariates to represent small-scale residual spatial variability, such that representing $g(\cdot)$ on the 36-km CMAQ grid is sufficient, based on posterior assessment of the scale of $g(\cdot)$. To calculate the PM likelihood I used the covariate values for the four km grid cell that each observation falls in, while using the value of \mathbf{g} from the 36 km grid cell the observation falls in. For the CMAQ likelihood, the CMAQ value for a given 36 km grid cell was related to the covariate effects on the four km grid by weighted averaging, with weights based on the overlap between a CMAQ grid cell and the four km grid cells.

I found that β_1 was estimated to be large (between 3 and 7), with ϕ strongly negatively correlated with \mathbf{L} and with ϕ having very large negative values to offset the large positive values of $\beta_1\mathbf{L}$. This appeared to be driven by the CMAQ model’s overprediction in some urban areas, with CMAQ estimating the urban to rural gradient as being much stronger than apparent in the observations. ϕ then adjusts for the effects (through $\beta_1\mathbf{L}$) of large values of β_1 elsewhere in the spatial domain. To address this in an ad hoc manner and identify ϕ as the orthogonal variation in the proxy not accounted for in the latent process, I carried out an ad hoc orthogonalization of ϕ and \mathbf{L} within each step of the MCMC. While a formal orthogonality constraint on ϕ and \mathbf{L} is technically appealing, this simple approach was effective in practice, and predictive results were similar with and without the orthogonalization. Other approaches to the problem might involve letting β_1 vary with covariates such as population density or truncating the very high CMAQ predictions.

Using this orthogonalized specification, the estimated values of β_1 were generally near one, as one would hope (Fig. 4g), and in this larger domain, more of the variability in CMAQ at larger scales was associated with the latent process than variability at smaller scales, suggesting that CMAQ is better able to resolve regional variability than more local variability (Fig. 4d). This is consistent with the discrepancy surfaces shown in Fig. 7, where one can see that the model corrects for hotspots at the scale of states or portions of states that show no evidence of being real hotspots based on the observations, such as over Iowa/southern Minnesota and eastern North Carolina. Once again, use of CMAQ as a proxy did not improve predictive ability (Table 2). Predictive performance was better than in the mid-Atlantic domain because of the greater range of natural variability in PM over this much larger area. When I considered the use of meteorological variables, the relationships were often the opposite of those expected based on scientific grounds, while prediction was little affected, once again presumably because of identifiability issues with respect to the residual spatial term, \mathbf{g} .

As a final assessment, I included CMAQ as a simple regression term, finding the cross-validation R^2 (RMSPE) to be 0.849 (1.60) for monthly prediction and 0.849 (1.05) for yearly prediction, both slightly better than modeling without the proxy (Table 2) but suggesting that there is limited additional information given the other terms in the model. Similarly modest improvements were seen when restricting to more rural sites. The posterior mean regression coefficients for CMAQ-estimated PM were between 0.48 and 0.89 for the 12 months, with the average of those 12 posterior

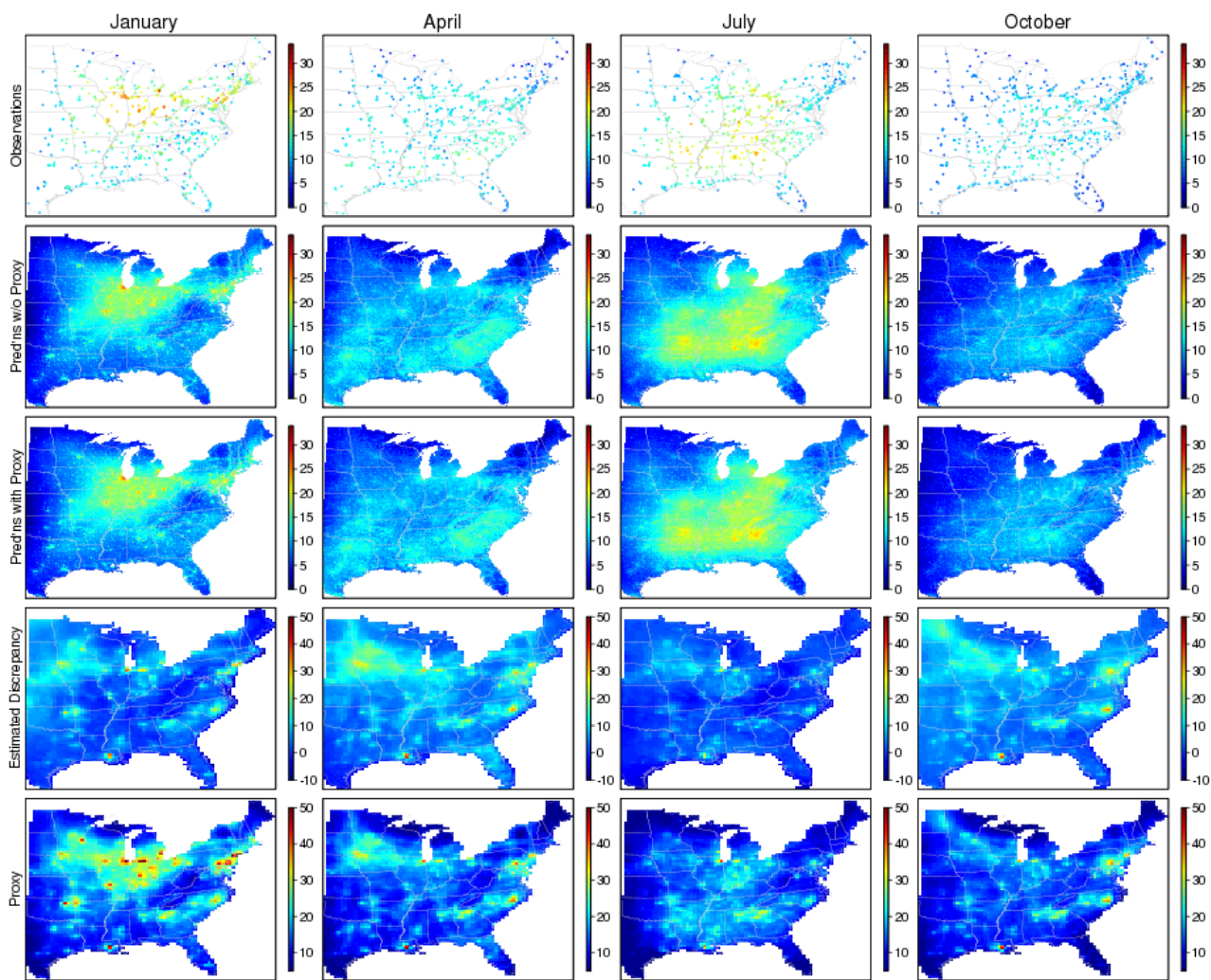


Figure 7: PM observations (first row), model PM predictions, excluding CMAQ (second row), model predictions including CMAQ (third row), estimated CMAQ discrepancy (fourth row), and CMAQ values (fifth row) for four months in 2001: January, April, July, and October (columns). Note that in January, some CMAQ values larger than $50 \mu\text{g}/\text{m}^3$ (up to $75 \mu\text{g}/\text{m}^3$) are truncated to $50 \mu\text{g}/\text{m}^3$.

means being 0.67.

I also considered whether CMAQ might be more helpful a setting with sparse observations (such as seen in the simulations) by artificially using only 100 monitors as the PM dataset, but found that prediction for the remaining monitor locations was very poor because with sparse PM observations I was not able to adjust for the CMAQ discrepancy as well as with more dense data. As above, including CMAQ as a regressor in this case did help to improve prediction slightly compared to a model that made use only of the observations.

5 Discussion

The model developed here is a spatial latent variable model, in which the proxy is decomposed into signal for the process of interest and noise, which raises the obvious concern of identifiability. Sufficient gold standard observations are required for the implicit calibration of the proxy relative to the observations that is done within the model. I fit a penalized model that identifies the discrepancy and the focal process based on a tradeoff between goodness of fit for the observations and for the proxy values and penalization of the latent spatial processes. This tradeoff is likely quite sensitive to model specification and to the relative richness of observation and proxy data. Indeed the differences in predictive ability for the spatial versus spatio-temporal models of Section 4.2 and the need for orthogonalization in Section 4.3 point to such sensitivity. In the examples, the model was not able to take advantage of the proxy data to improve predictive performance. Given that in the simulations, there was real signal that the model did not take advantage of, it is possible this is also occurring in the examples.

Despite these concerns about identifiability and sensitivity to model structure, my view is that this decomposition is a fundamental task when using proxies. One doesn't know the quality of the proxy and must assess this, ideally as a function of scale. A priori constraints on the flexibility of the discrepancy process incorporated into current data fusion approaches make strong assumptions about proxy quality. Such assumptions could contribute to overoptimism about the usefulness of proxy information and about the degree of certainty in resulting data fusion predictions. The model presented here attempts to assess proxy quality and to make use of available information in the proxy without prejudging that spatial correlation in the proxy reflects spatial signal in the process of interest.

The model accounts for errors and local variability in the observations, as well as spatial and temporal misalignment between observations and proxy. This should help in avoiding concluding that a proxy is not helpful because of noise or fine-scale variability in the 'gold standard', but I cannot completely rule out this possibility. However, I note that comparisons of daily maps of proxy values and observations indicate a great deal of mismatch between the two, of particular note on days when the observations show large-scale variation but little local variation. On such days the patterns in true PM are well-identified from the observations, yet the proxies often did a poor job of capturing that variation. It is possible that the proxy variables might add useful information in the absence of the GIS-based covariates, but part of the purpose of the covariates is to account for local variation in the observations that contributes to discrepancy between proxy and observations. Local variation that is not accounted for in the model structure is likely to mask any real relationship between the proxy and the true process of interest at the grid scale and may lead to discounting real information in the proxy.

In the space-time modeling, I use a simple space-time structure with the discrepancy process exchangeable across months but no month to month temporal correlation, but also suggest an AR(1) structure as equally feasible. Berrocal et al. (2009) and Sahu et al. (2009) specify independence for their analogous latent processes, while McMillan et al. (2010) use a spatio-temporal b-spline basis. As seen in the results, dependence between months does influence the estimation, with poorer predictive performance, suggesting that a simpler spatial model that is more straightforward to fit, interpret, and understand may be a better choice, despite not capturing all the temporal dependence in the data.

The approach here treats proxy information as data with an additional likelihood, extending Fuentes and Raftery (2005). Berrocal et al. (2009) proposed instead to regress on the proxy. In the simulations, I found that regressing on the proxy in some cases improved predictive ability and never decreased it relative to the two-likelihood models, with the added advantage of greatly reduced computational complexity. So if one is purely interested in prediction and not in understanding the structure of the proxy, a simple regression approach may be best. An important drawback is that for proxies such as remote sensing retrievals affected by cloud cover, missing observations are a problem. This then requires an imputation of some sort, bringing one back to modeling the proxy.

The second potential drawback is more subtle and involves difficulties in decomposing the proxy into scales when the relationship with the process of interest varies by scale. If the proxy captures small-scale patterns well, but misses large-scale patterns, then the additive spatial process term used in Berrocal et al. (2009) can adjust for this discrepancy, leveraging the proxy to improve prediction of small-scale variation. The potential concern arises when the proxy captures large-scale patterns well, but the small-scale patterns in the proxy are predominantly noise with respect to the process of interest, a likely scenario in applications. In such a setting, the model is likely to estimate a large regression coefficient for the proxy because of the large-scale association. The resulting prediction will be reasonable at the large scale but will also include all the small-scale spatial discrepancy in the proxy, which will be interpreted by the analyst as signal, with the proxy assumed to be of high quality at small scales. The spatial discrepancy term in the model will not be able to correct for this small-scale discrepancy because the data sparsity in the observations doesn't allow for estimation of and adjustment for this discrepancy. In such a situation I'd like to carry out a decomposition of the scales of variability in the proxy, but the regression approach conditions on all the scales of the proxy. Alternatively, the small-scale discrepancy in the proxy may act as measurement error, causing attenuation in the regression coefficient, potentially to near zero, limiting any information gain from the large-scale correspondence between proxy and process of interest.

From an interpretation standpoint, the proposed approach cleanly distinguishes between discrepancy and signal, at least in principle. A simpler alternative would be to explicitly decompose the proxy into two or more scales and include each component as a separate regression term, allowing the model to learn which scales are correlated with the observations. How to do this decomposition is an open question, but a simple approach would be to successively smooth the proxy with spatial smooth terms with fixed degrees of freedom.

Acknowledgements

I thank Yang Liu for processing the MODIS AOD and CMAQ output, as well as for collaboration on the overall project that led to this work, and Steve Melly for GIS processing. I thank Atmospheric and Environmental Research and the Electric Power Research Institute for providing the CMAQ output. NARR data were provided by the NOAA/OAR/ESRL PSD, Boulder, Colorado, from their web site at <http://www.cdc.noaa.gov>. This work was supported by grant 4746-RFA05-2/06-7 from the Health Effects Institute

References

- Andrieu, C. and J. Thoms (2008). A tutorial on adaptive MCMC. *Statistics and Computing* 18(4), 343–373.
- Banerjee, S., A. Gelfand, A. Finley, and H. Sang (2008). Gaussian predictive process models for large spatial data sets. *Journal of the Royal Statistical Society: Series B (Statistical Methodology)* 70(4), 825–848.
- Berrocal, V., A. Gelfand, and D. Holland (2009). A Spatio-Temporal Downscaler for Output From Numerical Models. *Journal of Agricultural, Biological, and Environmental Statistics* 15, 176–197.
- Besag, J. and D. Mondal (2005). First-order intrinsic autoregressions and the de Wijs process. *Biometrika* 92(4), 909–920.
- Crainiceanu, C., D. Ruppert, and M. Wand (2005). Bayesian analysis for penalized spline regression using WinBUGS. *Journal of Statistical Software* 14(14), 1–24.
- Draper, D. and M. Krnjacic (2006). Bayesian model specification. Technical report, Department of Applied Mathematics and Statistics, University of California Santa Cruz.
- Fuentes, M. and A. Raftery (2005). Model evaluation and spatial interpolation by Bayesian combination of observations with outputs from numerical models. *Biometrics* 61(1), 36–45.
- Fuentes, M., B. Reich, and G. Lee (2008). Spatial-temporal mesoscale modelling of rainfall intensity using gauge and radar data. *Annals of Applied Statistics* 2, 1148–1169.
- Gelman, A. (2006). Prior distributions for variance parameters in hierarchical models (comment on article by Browne and Draper). *Bayesian Analysis* 1(3), 515–534.
- Jun, M. and M. Stein (2004). Statistical comparison of observed and CMAQ modeled daily sulfate levels. *Atmospheric Environment* 38(27), 4427–4436.
- Kamman, E. and M. Wand (2003). Geoaddivitive models. *Applied Statistics* 52, 1–18.
- McMillan, N., D. Holland, M. Morara, and J. Feng (2010). Combining numerical model output and particulate data using Bayesian space-time modeling. *Environmetrics* 21, 48–65.

- Mugglin, A., B. Carlin, and A. Gelfand (2000). Fully model-based approaches for spatially misaligned data. *Journal of the American Statistical Association* 95(451), 877–887.
- Paciorek, C. (2007). Bayesian smoothing with Gaussian processes using Fourier basis functions in the spectralGP package. *Journal of Statistical Software* 19, 2.
- Paciorek, C. and Y. Liu (2009). Limitations of remotely-sensed aerosol as a spatial proxy for fine particulate matter. *Environmental Health Perspectives* 117, 904–909.
- Paciorek, C. and Y. Liu (submitted). Assessment and statistical modeling of the relationship between remotely-sensed aerosol optical depth and PM_{2.5}. Technical Report, Health Effects Institute Research Report.
- Paciorek, C., Y. Liu, H. Moreno-Macias, and S. Kondragunta (2008). Spatio-temporal associations between GOES aerosol optical depth retrievals and ground-level PM_{2.5}. *Environmental Science and Technology* 42, 5800–5806.
- Paciorek, C., J. Yanosky, R. Puett, F. Laden, and H. Suh (2009). Practical large-scale spatio-temporal modeling of particulate matter concentrations. *Annals of Applied Statistics* 3, 369–396.
- Rue, H. and L. Held (2005). *Gaussian Markov Random Fields: Theory and Applications*. Boca Raton: Chapman & Hall.
- Ruppert, D., M. Wand, and R. Carroll (2003). *Semiparametric Regression*. Cambridge, U.K.: Cambridge University Press.
- Sahu, S., A. Gelfand, and D. Holland (2009). Fusing point and areal level space-time data with application to wet deposition. *Journal of the Royal Statistical Society: Series C (Applied Statistics)* 59, 77–103.
- Silverman, B. (1984). Spline smoothing: the equivalent variable kernel method. *Annals of Statistics* 12(3), 898–916.
- Smith, R., S. Kolenikov, and L. Cox (2003). Spatiotemporal modeling of PM_{2.5} data with missing values. *Journal of Geophysical Research* 108, D9004.
- Sollich, P. and C. Williams (2005). Using the equivalent kernel to understand Gaussian Process regression. In *Advances in Neural Information Processing Systems 17*, pp. 1313–1320. MIT Press.
- Stein, M. and D. Fang (1997). Discussion of ozone exposure and population density in Harris County, Texas, by R.J. Carroll et al. *Journal of the American Statistical Association* 92, 408–411.
- Szpiro, A., P. Sampson, L. Sheppard, T. Lumley, S. Adar, and J. Kaufman (2009). Predicting intra-urban variation in air pollution concentrations with complex spatio-temporal dependencies. *Environmetrics*, in press.

Yanosky, J., C. Paciorek, and H. Suh (2009). Predicting chronic fine and coarse particulate exposures using spatio-temporal models for the northeastern and midwestern U.S. *Environmental Health Perspectives* 117, 522–529.

Yue, Y. and P. Speckman (2010). Nonstationary spatial Gaussian Markov random fields. *Journal of Computational and Graphical Statistics* 19, 96–116.

Appendix: Model structures and fitting details

Derivation of the MRF weight matrix for the thin plate spline approximation

Rue and Held (2005, Section 3.4.2) give a basic overview of the second-order, two-dimensional intrinsic Gaussian MRF that approximates a thin plate spline, but do not provide the details regarding the boundary condition effects that allow one to construct the full weight matrix, \mathbf{Q} . Here I provide the details, following the development in an unpublished manuscript by Y. Yue and P. Speckman, also given in Y. Yue’s unpublished Ph.D. dissertation from the Department of Statistics at the University of Missouri, Columbia.

A thin plate spline minimizes a penalized likelihood where the penalty term for a function, $g(\cdot)$, defined for $(s_1, s_2) \in \mathfrak{R}^2$ is

$$J(g) = \int \int_{\mathfrak{R}^2} \left[\left(\frac{\partial^2 g(s_1, s_2)}{\partial s_1^2} \right)^2 + 2 \left(\frac{\partial^2 g(s_1, s_2)}{\partial s_1 \partial s_2} \right)^2 + \left(\frac{\partial^2 g(s_1, s_2)}{\partial s_2^2} \right)^2 \right] ds_1 ds_2. \quad (3)$$

Taking the MRF as an approximation to $g(\cdot)$ on a regular grid of size $m_1 \times m_2$, a discretized approximation to $J(g)$ is

$$\sum_{i=3}^{m_1} \sum_{j=1}^{m_2} (\Delta_{s_1}^2 g_{i,j})^2 + 2 \sum_{i=2}^{m_1} \sum_{j=2}^{m_2} (\Delta_{s_1, s_2}^2 g_{i,j})^2 + \sum_{i=1}^{m_1} \sum_{j=3}^{m_2} (\Delta_{s_2}^2 g_{i,j})^2 \quad (4)$$

where

$$\begin{aligned} \Delta_{s_1}^2 g_{i,j} &= g_{i,j} - 2g_{i-1,j} + g_{i-2,j} \\ \Delta_{s_1, s_2}^2 g_{i,j} &= g_{ij} - g_{i-1,j} - (g_{i,j-1} - g_{i-1,j-1}) \\ \Delta_{s_2}^2 g_{i,j} &= g_{i,j} - 2g_{i,j-1} + g_{i,j-2}. \end{aligned}$$

$\Delta_{s_1}^2 g_{i,j}$ and $\Delta_{s_2}^2 g_{i,j}$ are the second order backward difference operators in the horizontal and vertical directions. $\Delta_{s_1, s_2}^2 g_{i,j}$ is found as the first order backward difference operator in the vertical direction applied to the first order backward difference operators in the horizontal direction.

The difference calculations are done for every cell on the grid and summed to approximate the integral in (3). Note that they cannot be calculated for cells on the lower and lefthand boundaries of the rectangular grid, nor can they be calculated for some of the terms for the cells in the second row from the bottom or second row from the left, hence some of the indices of summation in (4) do not start at one. Then to equate the elements of \mathbf{Q} with the coefficients of $\{g_{i,j}\}$ in (4), note that the discretized penalty can be expressed as $\mathbf{g}^\top \mathbf{Q} \mathbf{g} = \sum_{k=1}^m g_k^2 Q_{kk} + 2 \sum_{k=1}^m \sum_{l < k} g_k g_l Q_{kl}$ where

Spatial model structure

The basic model is a model with two likelihoods and additive mean terms, in particular

$$\begin{aligned}
\mathbf{Y} &\sim \mathcal{N}_{n_Y}(\mathbf{Z}_y \mathbf{b}_y + \mathbf{Z}_L \mathbf{b}_L + \mathbf{P}_\delta \boldsymbol{\delta}, \mathbf{V}_Y) \\
\mathbf{A} &\sim \mathcal{N}_{n_A}(\mathbf{P}_\phi \boldsymbol{\phi} + \mathbf{Z}_a \mathbf{b}_a + \beta_1 \mathbf{P}_A \mathbf{Z}_L \mathbf{b}_L, \mathbf{V}_A) \\
\boldsymbol{\delta} &\sim \mathcal{N}(\mathbf{0}, \sigma_h^2 \mathbf{I}) \\
\boldsymbol{\phi} &\sim \mathcal{N}_{m-3}(\mathbf{0}, (\kappa \mathbf{Q})^-) \\
\mathbf{b} = \{\mathbf{b}_y, \mathbf{b}_L, \mathbf{b}_a\} &\sim \mathcal{N}(\mathbf{0}, \boldsymbol{\Lambda})
\end{aligned}$$

where $\mathbf{Z}_y \mathbf{b}_y$ is the matrix representation of $\sum_p \beta_{y,p}(x_{y,p})$ and $\mathbf{Z}_L \mathbf{b}_L$ is the matrix representation of $\sum_p \beta_{L,p}(x_{L,p}) + g(s)$ with \mathbf{b}_L the collection of combined coefficients for the regression smooths and the spatial term, as well as including an intercept for \mathbf{Y} . Similarly, $\mathbf{Z}_a \mathbf{b}_a$ represents the influence of explanatory variables for the proxy unrelated to latent PM (cloud cover in the case of the AOD model). $\boldsymbol{\delta}$ are site-specific effects that account for correlation between monitors placed at the same site. I denote the variance of $\boldsymbol{\phi}$ using the generalized inverse to indicate that the prior is proper in an $m - 3$ dimensional space based on the construction of the TPS-MRF, fixing the mean and coefficients for linear terms of the spatial coordinates to zero. In the sampling, the three parameters are identified by the likelihood for \mathbf{A} , so I sample these parameters implicitly as part of $\boldsymbol{\phi}$ and therefore omit a separate intercept for \mathbf{A} . Given the limited number of observation locations, I use five knots for each regression smooth and 55 knots for the spatial residual. Knots were placed either uniformly over the range of covariate values or at equally-spaced quantiles to achieve reasonable spread over the covariate spaces, but given the use of penalized splines, results should be robust to the exact placement of knots. $\boldsymbol{\Lambda}$ is the prior covariance matrix of \mathbf{b} (non-informative for the fixed effect components and with exchangeable priors amongst the coefficients for a given regression smooth term, following Ruppert et al. (2003)).

I integrate over the conditional normal distribution of $\boldsymbol{\phi}$, with mean $\mathbf{M}_\phi = \mathbf{V}_\phi (\mathbf{P}_A^T \mathbf{V}_A^{-1} (\mathbf{A} - \mathbf{Z}_a \mathbf{b}_a - \mathbf{P}_A \mathbf{Z}_L \mathbf{b}_L))$ and variance $\mathbf{V}_\phi = (\mathbf{P}_\phi^T \mathbf{V}_A^{-1} \mathbf{P}_\phi + \kappa \mathbf{Q})^{-1}$ to obtain

$$\mathbf{A} \sim \mathcal{N}_{n_A-3}(\mathbf{Z}_a \mathbf{b}_a + \beta_1 \mathbf{P}_A \mathbf{Z}_L \mathbf{b}_L, \boldsymbol{\Sigma}_A).$$

Here $\boldsymbol{\Sigma}_A^{-1} = \mathbf{V}_A^{-1} - \mathbf{V}_A^{-1} \mathbf{P}_\phi \mathbf{V}_\phi \mathbf{P}_\phi^T \mathbf{V}_A^{-1}$ and $|\boldsymbol{\Sigma}_A|^{-\frac{1}{2}}$ can be expressed as

$$\frac{1}{|\boldsymbol{\Sigma}_A|^{\frac{1}{2}}} = \frac{\kappa^{\frac{m-3}{2}} |\mathbf{Q}|^{\frac{1}{2}}}{|\mathbf{V}_A|^{\frac{1}{2}} |\mathbf{V}_\phi^{-1}|^{\frac{1}{2}}}.$$

Note that the impropriety in the prior for $\boldsymbol{\phi}$ carries over into this marginal likelihood for \mathbf{A} , resulting in $m - 3$ rather than m in the exponent of κ and in $\boldsymbol{\Sigma}_A^{-1}$ being singular, with three zero eigenvalues, but the subsequent calculations all involve $\boldsymbol{\Sigma}_A^{-1}$ so no inversion is needed. Equivalently, I do not have a legitimate data-generating model for \mathbf{A} because of the prior impropriety. Information from three of the linear combinations in the quadratic form of the marginal likelihood contribute zero to the marginal likelihood because the variance for those combinations is infinite. I can avoid calculating the non-existent determinant of \mathbf{Q} because this is a constant with respect to the model parameters. Note that the impropriety is analogous to that in the marginal likelihood

obtained from integrating over the mean in a simple normal mean problem with an improper prior for the mean.

I can then integrate over the joint distribution for \mathbf{b} , where I construct \mathbf{Z}_Y and \mathbf{Z}_A such that $\mathbf{Z}_Y \mathbf{b} = \mathbf{Z}_y \mathbf{b}_y + \mathbf{Z}_L \mathbf{b}_L$ and $\mathbf{Z}_A \mathbf{b} = \mathbf{Z}_a \mathbf{b}_a + \mathbf{P}_A \mathbf{Z}_L \mathbf{b}_L$ by adding columns with all zeroes as necessary. The conditional distribution for \mathbf{b} is normal with mean, $\mathbf{M}_b = \mathbf{V}_b (\mathbf{Z}_Y^T \mathbf{V}_Y^{-1} (\mathbf{Y} - \mathbf{P}_\delta \boldsymbol{\delta}) + \mathbf{Z}_A^T \boldsymbol{\Sigma}_A^{-1} \mathbf{A})$ and $\mathbf{V}_b = (\mathbf{Z}_Y^T \mathbf{V}_Y^{-1} \mathbf{Z}_Y + \mathbf{Z}_A^T \boldsymbol{\Sigma}_A^{-1} \mathbf{Z}_A + \boldsymbol{\Lambda}^{-1})^{-1}$. I collect the remaining parameters as $\boldsymbol{\theta} = \{\beta_1, \sigma_{\text{sub}}^2, \sigma_\delta^2, \sigma_\epsilon^2, \sigma_A^2, \sigma_\alpha^2, \sigma_{b,L}^2, \sigma_{b,a}^2, \sigma_{b,y}^2, \kappa\}$ where the variance components, $\sigma_{b,y}^2$, $\sigma_{b,L}^2$, and $\sigma_{b,a}^2$, are vectors with one variance component for each smooth regression term in a given sum of regression smooths and σ_{sub}^2 , σ_δ^2 , σ_ϵ^2 , σ_A^2 , and σ_α^2 are parameters used to construct \mathbf{V}_Y and \mathbf{V}_A , described below. The marginal posterior for the remaining parameters and $\boldsymbol{\delta}$ is

$$P(\boldsymbol{\theta}, \boldsymbol{\delta} | \mathbf{A}, \mathbf{Y}) \propto |\boldsymbol{\Lambda}|^{-\frac{1}{2}} |\mathbf{V}_Y|^{-\frac{1}{2}} |\boldsymbol{\Sigma}_A|^{-\frac{1}{2}} |\mathbf{V}_b|^{\frac{1}{2}} P(\boldsymbol{\delta}) P(\boldsymbol{\theta}) \cdot \exp\left(-\frac{1}{2}((\mathbf{Y} - \mathbf{P}_\delta \boldsymbol{\delta})^T \mathbf{V}_Y^{-1} (\mathbf{Y} - \mathbf{P}_\delta \boldsymbol{\delta}) + \mathbf{A}^T \boldsymbol{\Sigma}_A^{-1} \mathbf{A} - \mathbf{M}_b^T \mathbf{V}_b^{-1} \mathbf{M}_b)\right), \quad (5)$$

which I use to sample $\boldsymbol{\theta}$ via blocked Metropolis. Depending on the model, in some cases I use a single block and in other cases subblocks. I use adaptive MCMC to tune the proposal covariance matrix throughout the chain (Andrieu and Thoms, 2008).

The key computational impediments involve the determinant of \mathbf{V}_ϕ^{-1} , which can be calculated based on sparse matrix operations since both of its components are sparse; note that \mathbf{P}_ϕ is a simple sparse mapping matrix assigning elements of ϕ to the proxy values. Next \mathbf{V}_b is a dense matrix whose size corresponds to the number of basis coefficients, which can be computationally burdensome when I use a large number of knots for \mathbf{g} or the total number of knots used for all the regression smooth terms is large. Finally, I must compute $\boldsymbol{\Sigma}_A^{-1} \mathbf{A}$ and $\boldsymbol{\Sigma}_A^{-1} \mathbf{Z}_A$, the latter being more burdensome because \mathbf{Z}_A is a matrix with as many non-zero columns as there are coefficients in $\{\mathbf{b}_a, \mathbf{b}_L\}$. Considering the representation of $\boldsymbol{\Sigma}_A^{-1}$, note that I can easily compute $\mathbf{V}_A^{-1} \mathbf{Z}_A$ and then $\mathbf{P}_\phi^T \mathbf{V}_A^{-1} \mathbf{Z}_A$ because \mathbf{V}_A^{-1} is diagonal and \mathbf{P}_ϕ^T is sparse. Next I use sparse matrix operations to solve the system of equations $\mathbf{V}_\phi \mathbf{P}_\phi^T \mathbf{V}_A^{-1} \mathbf{Z}_A$ (recall that I calculate \mathbf{V}_ϕ^{-1} quickly as the sparse matrix sum of two sparse matrices). I use the spam package in R for sparse matrix calculations.

Given the posterior for the remaining parameters (5), I can derive the closed form normal conditional distribution for $\boldsymbol{\delta}$, which has mean and variance,

$$\begin{aligned} \mathbf{M}_\delta &= \mathbf{V}_\delta (\mathbf{P}_\delta^T \mathbf{V}_Y^{-1} \mathbf{Y} - \mathbf{P}_\delta^T \mathbf{V}_Y^{-1} \mathbf{Z}_Y \mathbf{V}_b (\mathbf{Z}_Y^T \mathbf{V}_Y^{-1} \mathbf{Y} + \mathbf{Z}_A^T \boldsymbol{\Sigma}_A^{-1} \mathbf{A})) \\ \mathbf{V}_\delta^{-1} &= \sigma_\delta^2 \mathbf{i} + \mathbf{P}_\delta^T \mathbf{V}_Y^{-1} \mathbf{P}_\delta - \mathbf{P}_\delta^T \mathbf{V}_Y^{-1} \mathbf{Z}_Y \mathbf{V}_b \mathbf{Z}_Y^T \mathbf{V}_Y^{-1} \mathbf{P}_\delta. \end{aligned}$$

Sampling from this distribution efficiently involves sparse matrix calculations similar to those just described.

Posterior samples of ϕ and \mathbf{b} can be drawn off-line from the conditional distributions indicated above; I choose to draw them every 10 MCMC iterations.

\mathbf{V}_Y is modeled using a diagonal heteroscedastic variance, $(\mathbf{V}_Y)_{ii} = \sigma_\epsilon^2/n_i + k(n_i)\sigma_{\text{sub}}^2$ where the first term is the variance of the sum of independent daily instrument errors. The second reflects subsampling variability in the average of n_i instrument-error-free daily values relative to the average of the error-free daily values over all the days in the month, $\text{Var}(\sum_{d \in \text{subsample}} L_{i,d}/n_i - \sum_d L_{i,d}/n_{\text{month}})$, under the simplifying assumption of independence between true daily pollution values, $L_{i,d} \stackrel{iid}{\sim} \mathcal{N}(L(\mathbf{s}_i), \sigma_{\text{sub}}^2)$, which gives $k(n_i) = \frac{1}{n_i} - \frac{1}{n_{\text{month}}}$, where n_{month} is the number of days

in the month. Note that for simplicity I fixed σ_ϵ^2 at $\widehat{\sigma_\epsilon^2} = 1.5$, estimated in advance from co-located monitors, to enhance identifiability and because it has a small contribution to the overall error variance. For monitors not co-located with another monitor, I integrated over the prior for the δ values for those sites, which added a term, σ_h^2 , to $(\mathbf{V}_Y)_{ii}$. In contrast, I sampled the values of δ for sites with co-located monitors within the primary MCMC to avoid introducing off-diagonal elements into \mathbf{V}_Y as this would have obviated some of the computational efficiencies in the calculations outlined above. For models involving CMAQ, which is available for all days, I take $\mathbf{V}_A = \sigma_A^2 \mathbf{I}$. For models involving AOD, I use a diagonal heteroscedastic variance analogous to \mathbf{V}_Y that reflects the number of daily values in each monthly average, plus a homoscedastic term reflecting the fundamental discrepancy between AOD and true PM: $(\mathbf{V}_A)_{ii} = \sigma_A^2 + k(n_i)\sigma_\alpha^2$.

I use several covariates calculated for individual cells at the four km grid level: elevation at the cell centroids, population density, and total length of roads in three road classes. Area PM emissions from the 2002 EPA National Emissions Inventory (NEI) are calculated as density of emissions per county and the value for the county of the grid cell centroid is assigned to the grid cell. Population density, road density, and area emissions are log-transformed to reduce sparsity and pull in extremely large values in the right tail, and I truncated the values of some outlying covariates to reduce extrapolation problems. I used the NEI point source emissions strength and location data in the flexible buffer modeling described in Appendix D of Paciorek and Liu (submitted), creating a basis matrix that contributes columns to \mathbf{Z}_L . This matrix leverages the additive structure of the mixed model representation of a spline term to represent the effect of multiple point sources at a given receptor location (i.e., a monitor or prediction point) as the emission strength-weighted sum of a smooth distance effect evaluated for each individual source-receptor pair. The distance function is a universal function representing the effect of single source of unit strength on a receptor as a function of the distance between source and receptor, and is estimated from the data. I calculate the source strength-weighted sum of distance-weighted contributions from fine PM primary source point emissions within a maximum distance (100 km) for each monitor, omitting sources emitting less than five tons in 2002. For the proxy likelihood and for prediction on the grid, I take a subgrid of 16 points within each grid box and calculate the average sum of contributions from the point emissions within 100 km of the points in the subgrid, as a simple approximation to the true integral of the point emission effect over the grid cell.

Some CMAQ pixels overlap four km cells entirely over water, and those cells have undefined covariate values. I treat the CMAQ value in a CMAQ pixel as reflecting the weighted average of $L(\cdot)$ from only the land-based four km grid cells, with weights in \mathbf{P}_A summing to one for each CMAQ pixel. Exploratory analysis indicated that CMAQ-estimated PM in pixels on the land-water boundary was often high, such that not normalizing the weights to sum to one distorted the model fitting. The problem is that not normalizing reduces the contribution from \mathbf{L} to the mean of the CMAQ proxy, increasing the discrepancy between the proxy values and \mathbf{L} in cases (such as the New York City area) where the CMAQ proxy is very large. I do not include CMAQ values in the likelihood for CMAQ pixels with 60% or more overlap with four km cells that do not intersect land in the U.S.

In general, the prior distributions for hyperparameters were non-informative, with normal priors with large variances (and also lower and upper bounds to prevent the MCMC from wandering in flat parts of the posterior) for location parameters and uniform priors on the standard deviation scale for scale parameters (Gelman, 2006), with large upper bounds. In all cases, the posterior distributions were much more peaked than the prior distributions and away from the bounds, ex-

cept for some of the variance components for the coefficients of the regression smooths, which I restricted to avoid overly wiggly smooth terms. Further exploration of why these smooths tend toward less smooth functions than expected scientifically and on whether simple linear relationships would suffice, and might even improve out-of-sample prediction, would be worthwhile.

I ran the MCMC for 10,000 iterations during the burn-in and 25,000 subsequently, retaining every 10th iteration to reduce storage costs. I found reasonable convergence and mixing based on effective sample size calculations and trace plots. I did not run multiple chains for each month-validation set pair because of my use of multiple months and validation sets, noting that predictive performance also helps to justify the adequacy of the fitting.

Spatio-temporal model structure

The spatio-temporal model structure builds on the spatial model structure but with autoregressive structure for the basis coefficients, $\mathbf{b}_{g,t}$, $t = 1, \dots, T = 12$, of the monthly spatial residual surfaces, $g_t(\cdot)$, and an exchangeable structure for monthly discrepancy terms, ϕ_t , $t = 1, \dots, 12$, as well as month-specific $\beta_{1,t}$ with independent non-informative priors. Calculations based on sparse matrix routines follow those described for the spatial model but with $\mathbf{D} \otimes \mathbf{Q}$ in place of $\kappa\mathbf{Q}$. Because of the increase in dimensionality, it is difficult to work with grids as large as in the spatial model. In Section X, I fit the spatio-temporal model based on the 19×11 CMAQ grid, giving a $19 \times 11 \times 12 = 2508$ -dimensional ϕ . A major cause of slowdown is that the \mathbf{b} vector is now much higher dimensional, as it includes $55 \times 12 = 660$ basis coefficients for the 12 residual spatial surfaces. Given the increase in sample size (albeit the same number of locations), I use 10 rather than 5 knots for the regression smooth terms, allowing for the possibility of estimating additional nonlinearity. I ran the MCMC for 10,000 iterations during the burn-in and 50,000 subsequently, retaining every 10th iteration to reduce storage costs, again finding reasonable convergence and mixing.

Subnational model structure

Spatio-temporal modeling of small-scale spatial variation for the eastern U.S. is computationally challenging, so I fit separate spatial models for each month. I represent ϕ and \mathbf{g} as TPS-MRFs on the $73 \times 77 = 5621$ dimensional CMAQ grid over the eastern U.S., each with its own precision parameter. Covariate effects are represented on the original four km base grid (now of dimension $669 \times 677 = 452,913$). Pre-computation of \mathbf{Z}_A in advance of the MCMC involves the large matrix multiplication of a basis matrix and an averaging matrix that represents the weighted average of four km cells within each CMAQ pixel based on the amount of overlap. \mathbf{Z}_Y also represents the product of a mapping matrix and the original basis matrices for the covariates. Given the relatively large sample size, for this model I again use 10 rather than five knots for each regression smooth term.

The initial integration is over $\phi^* = \{\mathbf{g}, \phi\}$ followed by integration over \mathbf{b} , which no longer includes \mathbf{b}_g . The first integration is done by representing the joint likelihood as

$$\begin{pmatrix} \mathbf{Y} \\ \mathbf{A} \end{pmatrix} \sim \mathcal{N}_{n_Y+n_A} \left(\begin{pmatrix} \mathbf{Z}_Y \\ \mathbf{Z}_A \end{pmatrix} \mathbf{b} + \begin{pmatrix} \mathbf{P}_Y & \mathbf{0} \\ \beta_1 \mathbf{P}_A & \mathbf{P}_A \end{pmatrix} \begin{pmatrix} \mathbf{g} \\ \phi \end{pmatrix} + \begin{pmatrix} \mathbf{P}_\delta \\ \mathbf{0} \end{pmatrix} \delta, \begin{pmatrix} \mathbf{V}_Y & \mathbf{0} \\ \mathbf{0} & \mathbf{V}_A \end{pmatrix} \right),$$

followed by analogous calculations as in the original spatial model to integrate over \mathbf{b} and determine the marginal posterior (up to the normalizing constant) for the remaining parameters and the

conditional normal posterior for δ given the remaining parameters and the data. Note that P_Y and P_A simply map from the CMAQ grid cells to the observations and CMAQ values.

For the point source emissions covariate, computational demands required that I consider only point sources emitting more than 10 tons per year within 50 km of a given location, with the integral approximation using a subgrid with four, rather than 16, points within each four km cell.

I ran the MCMC for 10,000 iterations during the burn-in and 20,000 subsequently, retaining every 10th iteration to reduce storage costs, again finding reasonable convergence and mixing.